

Cite this article as: Yuan Xiangsheng, Gao Chunping, Luo Tiegang, et al. Effect of YbB₆ on Microstructure and Mechanical Properties of Ti-6Al-4V Titanium Alloy[J]. Rare Metal Materials and Engineering, 2022, 51(07): 2361-2369.

ARTICLE

Effect of YbB₆ on Microstructure and Mechanical Properties of Ti-6Al-4V Titanium Alloy

Yuan Xiangsheng^{1,2}, Gao Chunping^{1,2}, Luo Tiegang^{1,3}, Zheng Xueping², Li Zhi^{1,3}, Yang Jie², Zheng Zimu², Zhang Jiawei², Luo Yuheng⁴

¹Institute of New Materials, Guangdong Academy of Sciences, Guangzhou 510650, China; ²School of Materials Science and Engineering, Chang'an University, Xi'an 710061, China; ³Guangdong Provincial Key Laboratory of Metal Toughening Technology and Application, Guangzhou 510650, China; ⁴School of Environmental and Chemical Engineering, Nanchang Hangkong University, Nanchang 330063, China

Abstract: The Ti-6Al-4V titanium alloy with YbB₆ addition was fabricated by spark plasma sintering (SPS), and the effects of YbB₆ addition on microstructure and mechanical properties of Ti-6Al-4V titanium alloy were investigated. The results show that with increasing the YbB₆ content, the microstructure of the composites is clearly changed, and the grains are obviously refined. The in-situ formation of TiB whiskers and Yb₂O₃ particles is beneficial to the improvement of mechanical properties of the composites. Furthermore, with the addition of 0.6wt% YbB₆, the relative density, microhardness, yield strength, ultimate tensile strength, and elongation of the sintered alloys are 99.43%, 4030 MPa, 903 MPa, 1148 MPa, and 3.3%, respectively. Compared to those of Ti-6Al-4V alloy, the aforementioned properties of the sintered alloys with 0.6wt% YbB₆ are increased by 0.37%, 13.8%, 38.07%, and 17.14%, respectively. The strengthening mechanism is mainly attributed to the microstructure transformation, grain refinement, and dispersion strengthening. With increasing the YbB₆ content, the fracture mode is the combination of ductile fracture and brittle fracture.

Key words: Ti-6Al-4V; YbB₆; spark plasma sintering; microstructure; mechanical properties

Titanium alloys are widely used in medical equipment, chemical industry, aerospace, and other fields due to their unique functions of good biocompatibility, outstanding corrosion resistance, high strength-to-weight ratio, and excellent shape memory ability^[1-6]. Ti-6Al-4V alloy is a typical dual-phase titanium alloy consisting of α and β phases with good mechanical properties^[7]. Nevertheless, the poor plasticity at room temperature, low hardness, and serious work hardening effect of Ti-6Al-4V titanium alloy all restrict its application^[8,9]. During the melting process, Pang et al^[10] found that Ti-6Al-4V titanium alloy can produce defect area with uneven chemical composition, which contains abundant oxygen and a small amount of Al and V, thereby forming the oxygen-rich inclusions. The defects and the formation of coarse phase structure both result in the decrease in microhardness and plasticity.

In order to solve these problems, the properties of titanium

alloys have been improved by optimizing the processes and adding reinforcement particles or fibers. The laser surface cladding, additive manufacturing, physical vapor deposition, and chemical vapor deposition were used to improve the mechanical properties of Ti-6Al-4V titanium alloy^[11,12]. Nevertheless, these methods also have their restrictions. For example, the films deposited on titanium alloys by physical and chemical vapor deposition methods are usually very thin and have poor adhesion to substrate^[12]. The spark plasma sintering (SPS) method has obvious advantages in film preparation^[13,14]: the materials prepared by SPS have uniform components and dense structure. Besides, SPS has the advantages of fast sintering rate, controllable structure, energy saving, and environmental protection^[15-18].

The particles or fibers have also been used to enhance the specific strength, specific modulus, and wear resistance of titanium alloys. The commonly used reinforcement phase

Received date: July 24, 2021

Foundation item: Guangdong Province Key Area R&D Program (2019B010942001); Guangzhou Science and Technology Project (201704030094); Sponsored by Guangdong Institute of Materials and Processing; Fundamental Research Funds for the Central Universities, CHD (300102310501); Jiangmen Project ([2020]182#)

Corresponding author: Luo Tiegang, Ph. D., Professor, Institute of New Materials, Guangdong Academy of Sciences, Guangzhou 510650, P. R. China, E-mail: luotiegang@gdinm.com

Copyright © 2022, Northwest Institute for Nonferrous Metal Research. Published by Science Press. All rights reserved.

includes the TiB, TiC, WC, Y₂O₃, and La₂O₃^[19-23]. The rare earth elements show outstanding performance as high-efficiency oxygen scavengers in titanium composites due to their high chemical affinity with oxygen. Bermingham et al^[24] showed that the maximum strength is increased by 10% when lanthanum hexaboride and boron are added into the composite. Yan et al^[25] found that adding yttrium hydride to Ti-2.25Mo-1.5Fe alloy can form the yttrium oxide and yttrium chloride, which greatly improves the alloy ductility.

In this research, 6 types of Ti-6Al-4V/YbB₆ composites were prepared by SPS. The effect of YbB₆ addition on the microstructures and mechanical properties of composites was investigated. In addition, the fracture mode of Ti-6Al-4V/YbB₆ composites was discussed.

1 Experiment

The main raw materials used in experiment were Ti-6Al-4V alloy powder (purity of 99.5%, particle size of 30~50 μm) and YbB₆ powder (purity of 99.5%, particle size of 20~30 μm). The composition of Ti-6Al-4V alloy powder is shown in Table 1. The raw materials were mixed according to the mixture ratio in Table 2 to prepare the Ti-6Al-4V/YbB₆ composites.

The raw materials were mixed by ball milling. In order to further refine the YbB₆ particles and to reduce the degree of agglomeration, the YbB₆ powders were firstly ball-milled in a planetary ball mill (QM-3SP4) under argon atmosphere. The ball-to-material ratio was 10:1, and the ball milling was performed at a milling speed of 200 r/min for 4 h. The Ti-6Al-4V alloy and YbB₆ powders were mixed at a ball milling ratio of 8:1 and milling speed of 300 r/min for 3 h. In order to minimize the oxidation, all mixing processes were conducted under the argon atmosphere. The mixed alloy powder was sintered in a high vacuum environment with the heating rate of 100 °C/min by SPS under the pressure of 30 MPa at 1100 °C for 5 min.

The phase components of the composites were analyzed by X-ray diffraction (XRD, D/max 2550) with Cu Kα. The scanning speed of XRD was 5°·min⁻¹, the step distance was 0.02°, and the range was 2θ=30°~80°. The optical microscope (OM), scanning electron microscope (SEM, JXA-8100)

Table 1 Chemical composition of Ti-6Al-4V alloy powder (wt%)

Al	V	O	N	C	Ti
6.43	4.0	0.13	0.06	0.01	Bal.

Table 2 Components of different Ti-6Al-4V/YbB₆ alloy specimens (wt%)

Specimen	YbB ₆	Ti-6Al-4V
B-0	0.0	100.0
B-2	0.2	99.8
B-4	0.4	99.6
B-6	0.6	99.4
B-8	0.8	99.2
B-10	1.0	99.0

equipped with energy dispersive spectrometer (EDS), and transmission electron microscope (TEM, JEOL-2100F) were used to study the microstructures of the composites.

The density of the polished as-sintered composites was measured by the Archimedes method, and then the microhardness was tested by the Vickers microhardness tester (ZHU-S) at a load of 3 N for 15 s. In order to obtain the accurate hardness of sintered composites, at least 9 positions with the distance of 4 mm were selected. The tensile tests were performed at room temperature by a universal testing machine (CMT-4024) at a constant strain rate of 1 mm/min. The specimens used for tensile tests were machined according to Fig. 1. The yield strength (MPa), ultimate tensile strength (MPa), and elongation (%) were measured. The fracture morphologies of the tensile specimens were observed by SEM.

2 Results and Discussion

2.1 Morphologies of powders

The morphologies of raw materials and mixed powders are shown in Fig. 2. It can be seen that the particle size of Ti-6Al-4V alloy powder is 15~45 μm. The Ti-6Al-4V alloy powder shows regular spherical morphology and the powder dispersion is relatively uniform. Fig. 2b shows that the particle size of YbB₆ powder is 10~50 μm, and these particles agglomerate with irregular shapes. Fig. 2c shows the morphology of the mixed powder of B-6 specimen. Fig. 2d shows the magnified microstructure of the rectangular area in Fig. 2c. It can be seen that the YbB₆ powder is evenly distributed on the surface of spherical Ti-6Al-4V powders, but there is a slightly uneven distribution in some positions. The morphology of the powder changes slightly after the ball milling.

2.2 Microstructures and phase constituents

Fig. 3 shows OM microstructures of different Ti-6Al-4V/YbB₆ alloys. It can be seen that the microstructure of Ti-6Al-4V alloy (B-0) is mainly the Widmanstatten structure consisting of α+β phases: the content of acicular α phase is high, and β phase is mainly distributed at the grain boundaries of α grains. When 0.2wt% YbB₆ is added, a few particles and whisker-like products begin to appear in the structure, and the microstructure is still mainly composed of lamellar α phase and intergranular β phase. Fig. 3c~3f show that with increasing the content of YbB₆, more and more particles and whisker-like

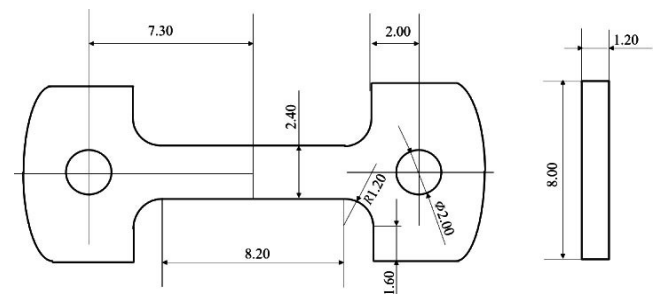


Fig.1 Schematic diagrams of tensile specimens

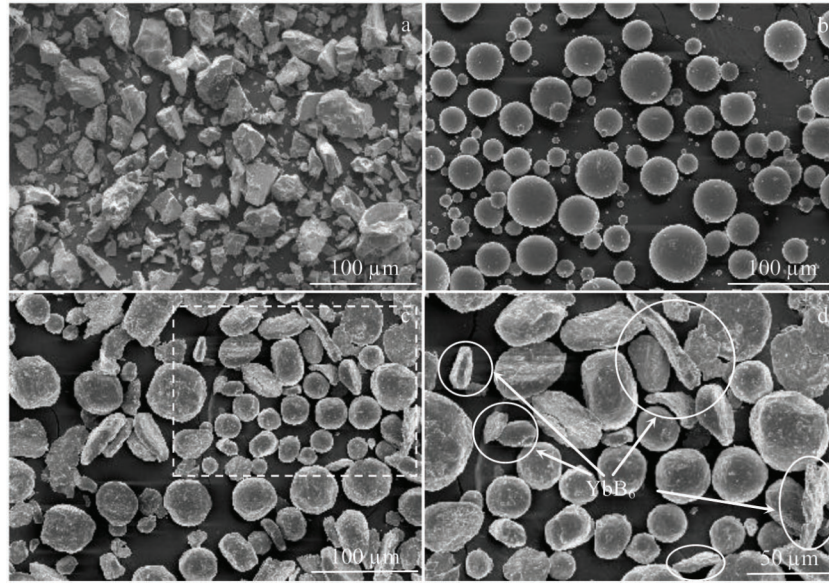


Fig.2 SEM morphologies of raw materials and mixed powders: (a) Ti-6Al-4V, (b) YbB_6 , and (c, d) mixed powder of B-6 specimen

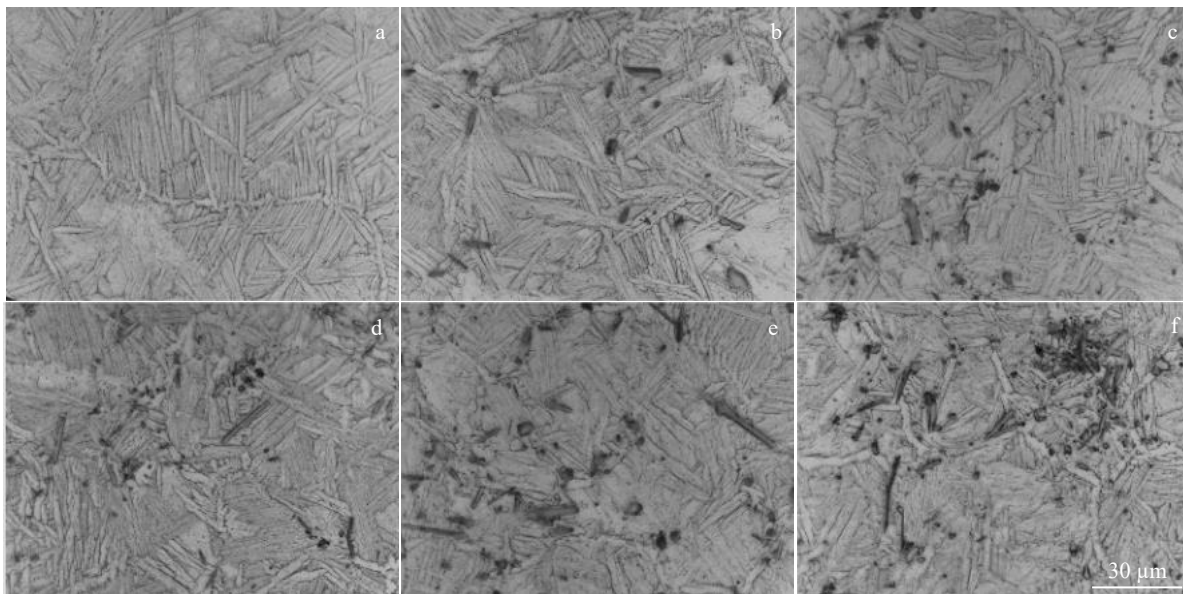


Fig.3 OM microstructures of different Ti-6Al-4V/ YbB_6 alloys: (a) B-0, (b) B-2, (c) B-4, (d) B-6, (e) B-8, and (f) B-10

products appear in the structure. However, when the YbB_6 is added excessively, the compounds prepared by in-situ reaction are distributed in a large area, which influences the microstructure to a certain extent. With increasing the YbB_6 content, the crystal microstructure is changed obviously. The initial length of α and β grains decreases, and the aspect ratio of α grain decreases, forming the flaky α and β phases. In addition, the initial acicular α phase decreases in content.

Table 3 shows the experiment densities and relative densities of as-sintered Ti-6Al-4V/ YbB_6 alloys. As the YbB_6 content increases, the density of the as-sintered Ti-6Al-4V/ YbB_6 alloy increases firstly and then decreases. When 0.6wt%

YbB_6 is added into the alloy, the optimal relative density of 99.43% can be achieved, which is increased by 0.37% compared with that of B-0 specimen. The main reason for this phenomenon is that the in-situ reaction occurs during the sintering process, thereby forming the TiB whiskers and Yb_2O_3 particles, which can purify the O element on the surface of Ti-6Al-4V powder. Besides, the newly generated reinforcement phase is also beneficial to increase the relative density.

Fig. 4 shows SEM microstructures of Ti-6Al-4V/ YbB_6 alloys. It can be seen that with increasing the YbB_6 content, the microstructure is changed. The holes or defects barely

Table 3 Experiment densities and relative densities of as-sintered Ti-6Al-4V/YbB₆ alloy specimens

Specimen	Experiment density/g·cm ⁻³	Relative density/%
B-0	4.4086±0.0092	99.06±0.21
B-2	4.4176±0.0095	99.27±0.22
B-4	4.4203±0.0112	99.33±0.25
B-6	4.4248±0.0102	99.43±0.23
B-8	4.4240±0.0089	99.41±0.21
B-10	4.4212±0.0108	99.35±0.24

exist in the sintered alloys, which is attributed to the higher density of the as-sintered specimen. With increasing the YbB₆ addition, the whisker-like TiB and Yb₂O₃ particle appear. During the sintering process, YbB₆ spontaneously forms the rare earth oxides through the decomposition process. When the rare earth elements are introduced into the liquid titanium matrix, the rare earth elements dissolve to form oxides, thereby removing O element. The B element produced by decomposition reacts with Ti to form TiB. When 0.2wt% YbB₆ is added into the alloy, some sparsely dispersed whisker-like TiB and small Yb₂O₃ particles can be observed. When 0.6wt% YbB₆ is added, the content of whisker-like TiB and Yb₂O₃ particles increases and these two components are uniformly dispersed. However, with further increasing the YbB₆ content, the products of the in-situ reaction accumulate and produce some defects, resulting in the decline in the alloy properties.

Fig. 5 shows SEM microstructure of the sintered B-6 specimen and the corresponding EDS element mapping of Ti, Al, V, Yb, B and O. The results show that Ti, Al, V, and O elements are evenly distributed, while B and Yb elements are

mainly distributed in the whisker-like structure and the particles, respectively. It can be seen that the TiB and Yb₂O₃ are generated. Due to the in-situ reaction, the Ti-6Al-4V alloy has a better deoxidizing effect during sintering, which is more conducive to material densification and can further improve its mechanical properties.

XRD patterns of the as-sintered Ti-6Al-4V/YbB₆ alloys are shown in Fig. 6. It can be seen that the phase composition is changed with different contents of YbB₆. As for the Ti-6Al-4V alloys with YbB₆ addition, the diffraction peaks of α -Ti, β -Ti, TiB, and Yb₂O₃ can be observed. It can be inferred that the in-situ reaction occurs during the sintering process to generate TiB and Yb₂O₃. It can also be found that with increasing the YbB₆ content, the diffraction peaks of TiB and Yb₂O₃ become more obvious.

TEM microstructures and the selected area electron diffraction (SAED) patterns of the B-6 specimen are shown in Fig. 7. It can be seen from Fig. 7a and 7b that when 0.6wt% YbB₆ is added to Ti-6Al-4V alloy, an in-situ reaction occurs: TiB and rare earth oxide Yb₂O₃ are formed. The Yb₂O₃ is mainly distributed in the grains to play a role of dispersion strengthening, and a small amount of Yb₂O₃ is distributed near the grain boundaries, which is beneficial to inhibit the grain growth and to further improve the performance of Ti-6Al-4V alloy. The generated TiB exists in the crystal grains in the form of long block and whisker, which greatly improves the alloy strength. Fig. 7b and 7c show that the interface between the compound produced by the in-situ reaction and the substrate is free of impurities, i. e., the bonding surface is clean. Thus, the generated in-situ product has good bonding with the alloy matrix.

Fig. 7d~7g show SAED patterns of TiB with alloy matrix,

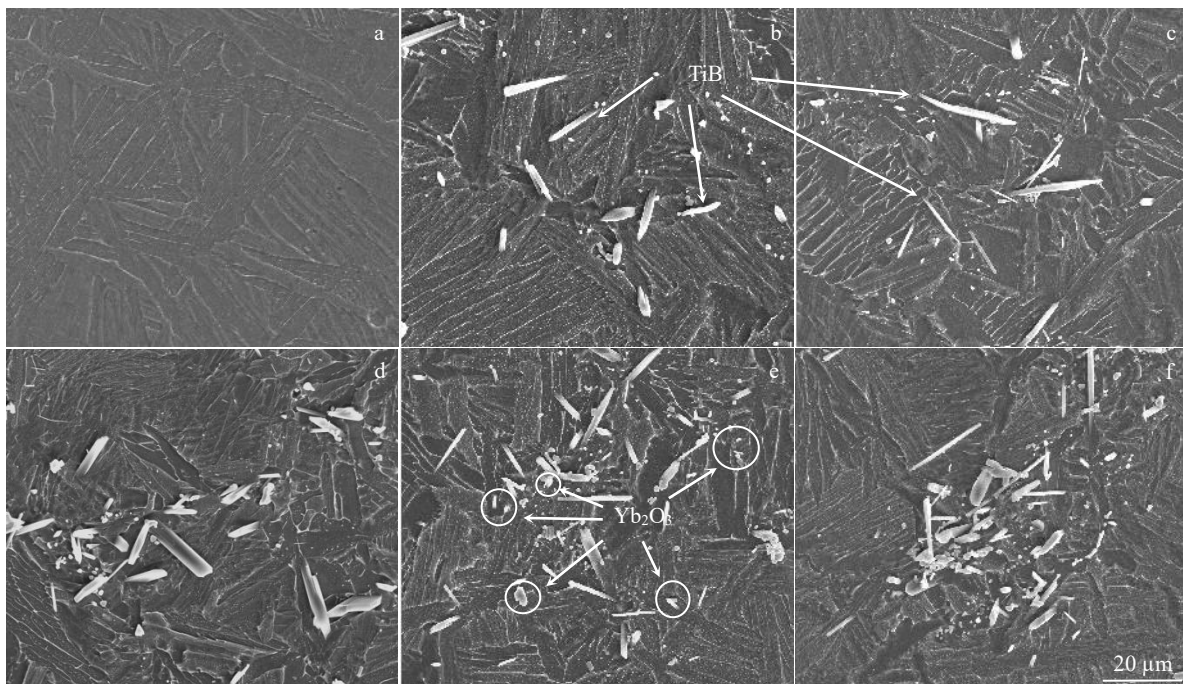


Fig. 4 SEM microstructures of different as-sintered Ti-6Al-4V/YbB₆ alloys: (a) B-0, (b) B-2, (c) B-4, (d) B-6, (e) B-8, and (f) B-10

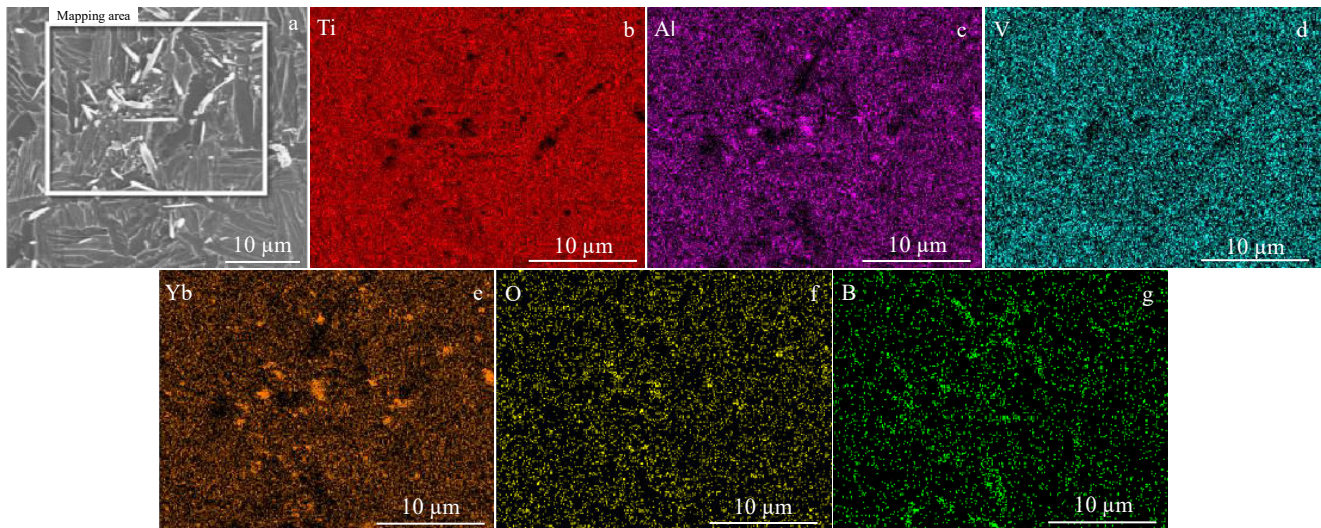


Fig.5 SEM microstructure (a) and EDS element mapping of Ti (b), Al (c), V (d), Yb (e), O (f), and B (g) of as-sintered B-6 specimen

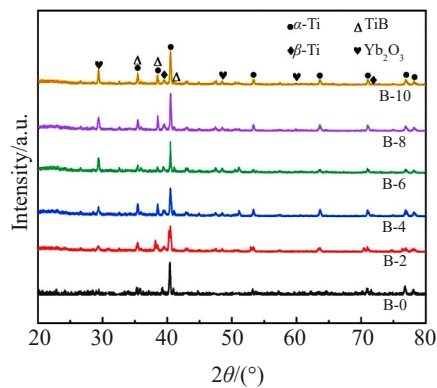


Fig.6 XRD patterns of different Ti-6Al-4V/YbB₆ alloys

α -Ti[0001], β -Ti[013], and Yb₂O₃[222], respectively. It can be found that TiB has a hexagonal close-packed (hcp) structure, and the whisker-like TiB has a hexagonal cross-section and exhibits a strong preferential growth along the B27[010] direction^[26]. The α -Ti also has an ordered hcp structure, and β -Ti has an ordered body-centered cubic (bcc) structure. In addition, EDS results in Fig.7h and 7i indicate that Point 1 and Point 2 are mainly composed of TiB and Yb₂O₃, respectively. According to above analyses, it can be concluded that the combination type of Ti and Yb₂O₃ is physical absorption. It can be seen that Yb₂O₃ contains a small amount of Ti due to the Ti-6Al-4V alloy matrix. These analysis results are consistent with SAED patterns, so it can be determined that Yb₂O₃ and TiB are generated during the sintering process, which is beneficial to the improvement of the mechanical properties of alloys.

2.3 Mechanical properties

In order to obtain the influence of YbB₆ content on mechanical properties of Ti-6Al-4V/YbB₆ alloys, the Vickers microhardness and tensile properties of all specimens were

measured, as shown in Fig.8 and Fig.9, respectively. It can be found that the microhardness of Ti-6Al-4V alloy without YbB₆ is 3540 MPa. The microhardness of the Ti-6Al-4V alloys is significantly improved after the YbB₆ addition. With increasing the YbB₆ content from 0.0wt% to 0.6wt%, the density of the prepared specimens becomes higher and the microhardness is increased. However, when the YbB₆ content exceeds 0.6wt%, the microhardness decreases. The maximum microhardness is 4030 MPa of the B-6 specimen, which is 13.8% higher than that of the pure Ti-6Al-4V alloy. With increasing the YbB₆ content, the change trend of microhardness agrees well with the microstructure transformation and the formation of reinforcement phase. With increasing the YbB₆ content, the number of newly formed reinforcement phases is increased until the accumulation of reaction product occurs. Menéndez et al^[27] found that the dislocation entanglement at the grain boundary in alloy of high relative density prevents the movement of dislocations and improves the deformation resistance, resulting in the increase in microhardness.

Fig.9 shows the mechanical properties of as-sintered Ti-6Al-4V/YbB₆ alloys. The yield strength, ultimate tensile strength, and elongation of Ti-6Al-4V alloy are 654 MPa, 980 MPa, and 2.5%, respectively. After the YbB₆ addition, the reinforcement particles (Yb₂O₃) and reinforcement phase (whisker-like TiB) are generated during the reaction in the Ti-6Al-4V/YbB₆ alloys, leading to higher yield strength and better tensile strength.

When 0.6wt% YbB₆ is added into the alloy, the maximum yield strength, maximum ultimate tensile strength, and maximum elongation of 903 MPa, 1148 MPa and 3.3% are achieved, respectively. The yield strength and ultimate tensile strength of B-6 specimen are increased by 38.07% and 17.14%, compared with those of B-0 specimen, respectively. The ultimate tensile strength is increased obviously. The

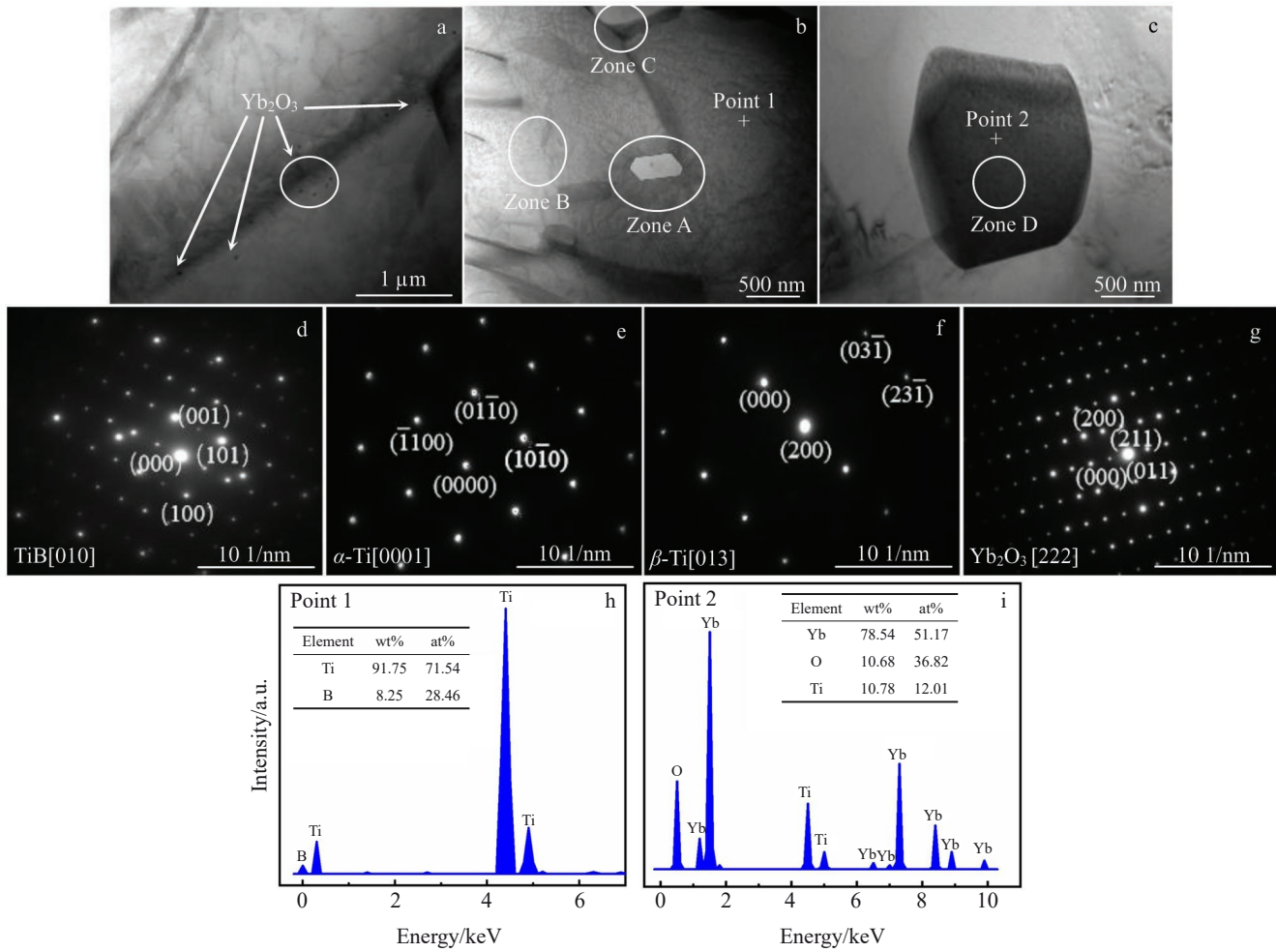


Fig.7 TEM bright field images of B-6 specimen foil (a-c); SAED patterns of Zone A~C in Fig.7b and Zone D in Fig.7c: (d) Zone A (TiB and alloy matrix), (e) Zone B (α -Ti), (f) Zone C (β -Ti), and (g) Zone D (Yb_2O_3); EDS results of Point 1 in Fig.7b (h) and Point 2 in Fig.7c (i)

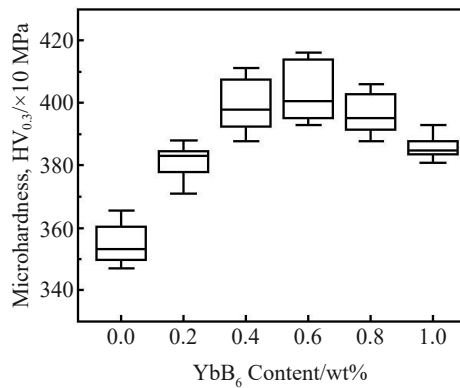


Fig.8 Microhardness of different Ti-6Al-4V/YbB₆ alloys

higher the density, the smaller the porosity, and the higher the tensile strength. However, when the YbB₆ content is 1.0wt%, the yield strength, ultimate tensile strength, and elongation decreases to 686 MPa, 1050 MPa, and 2.0%, respectively.

It can be found that the generated Yb₂O₃ particles are mainly distributed near the TiB, and some of them are

distributed in the crystal grains as the reinforcement particles. In addition, the microstructure is also changed from Widmanstatten structure to a structure mainly consisting of lamellar α phase and intergranular β phase with refined grains. The fine grains can shorten the slip surface, reduce the length of dislocation movement, and decrease the dislocation accumulation on the slip surface. The stress concentration at the interface between the slip surface and the grain boundary can also be released through the fine grains, which inhibits the crack formation, thereby leading to higher fracture strength. In this research, the Orowan strengthening and fine-grain strengthening can be used to explain the role of Yb₂O₃ in the strengthening mechanism of Ti-6Al-4V/YbB₆ alloys. The strengthening effect ($\Delta\sigma$) can be expressed as follows:

$$\Delta\sigma = \Delta\sigma_{H-P} + \Delta\sigma_{Orowan} \quad (1)$$

where $\Delta\sigma_{H-P}$ is the strengthening effect caused by Hall-Patch rule; $\Delta\sigma_{Orowan}$ is the strengthening effect caused by Orowan relationship. The strength of Ti-6Al-4V/YbB₆ alloys can obviously be enhanced by grain refinement. The strength increase can be calculated by Eq.(2), as follows:

$$\Delta\sigma_{H-P} = K(d_1^{-\frac{1}{2}} - d_2^{-\frac{1}{2}}) \quad (2)$$

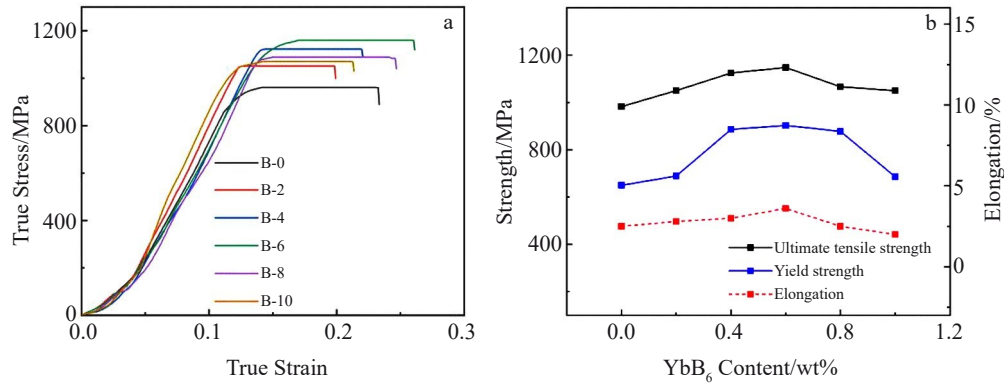


Fig.9 True stress-true strain curves (a) and mechanical properties (b) of different Ti-6Al-4V/YbB₆ alloys

where K is the strengthening coefficient of $0.91 \text{ MPa} \cdot \text{m}^{1/2}$ ^[28]; d_1 and d_2 represent the particle size before and after grain refinement, respectively.

$\Delta\sigma_{\text{Orowan}}$ is caused by the inhibition of dislocation movement by fine particles^[29], as follows:

$$\Delta\sigma_{\text{Orowan}} = \frac{0.13G|b|\ln(d/|b|)}{d_p \left[\left(\frac{1}{2V_p} \right)^{\frac{1}{3}} - 1 \right]} \quad (3)$$

where b represents the Burger vector of Ti-6Al-4V matrix; G represents the shear modulus of Ti-6Al-4V matrix; d , d_p , and V_p represent the average grain size of Ti-6Al-4V matrix, average particle radius of Yb₂O₃, and the volume fraction of Yb₂O₃ in matrix, respectively.

2.4 Fracture morphology

The tensile fracture morphologies of Ti-6Al-4V/YbB₆ alloys are shown in Fig. 10. It can be clearly seen that the

fracture morphology contains many dimples, and the fracture is mainly ductile and brittle fracture. Fig. 10a shows the typical ductile morphology of the sintered Ti-6Al-4V alloy^[30] with shallow dimples and some small micropores in the matrix.

As shown in Fig. 10b–10e, TiB and Yb₂O₃ particles can be observed. The Yb₂O₃ particles mainly exist in the fractured dimples. There are some small dimples on the edges, indicating that the presence of Yb₂O₃ plays an important role to improve the alloy plasticity. The formation of whisker-like TiB is beneficial to the increase in mechanical properties and has a certain effect on the tensile fracture morphology. When the YbB₆ content is increased from 0.0wt% to 0.6wt%, there are more and more dimples, whereas the number of micropores is reduced. However, when the YbB₆ content exceeds 0.6wt%, the dimples become smaller and shallower,

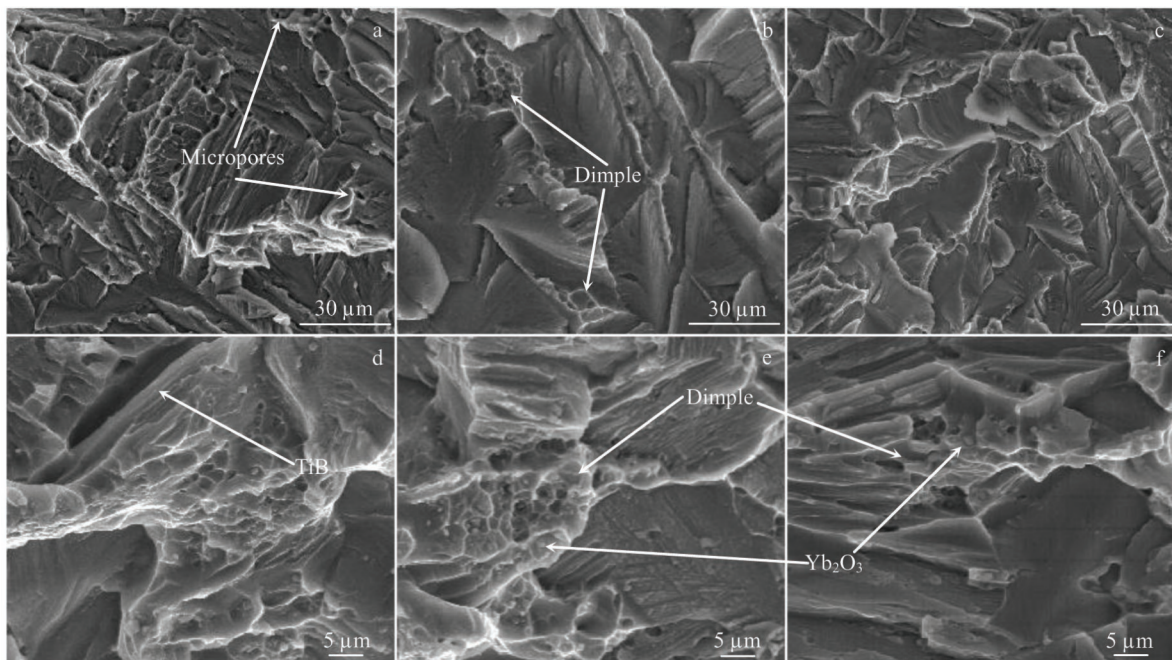


Fig.10 Tensile fracture morphologies of different as-sintered Ti-6Al-4V/YbB₆ alloys: (a) B-0, (b) B-2, (c) B-4, (d) B-6, (e) B-8, and (f) B-10

compared with those in the sintered B-6 specimen. The main reason for this phenomenon is that when the YbB_6 content increases, the probability of agglomeration of the Yb_2O_3 particles increases, which results in defects and lower plasticity.

3 Conclusions

1) With increasing the YbB_6 content, more and more reinforcement phases TiB and Yb_2O_3 are generated by the in-situ reaction in Ti-6Al-4V/ YbB_6 alloy during the spark plasma sintering (SPS), which is beneficial to the improvement in mechanical properties of Ti-6Al-4V titanium alloys.

2) The sintered Ti-6Al-4V alloy with 0.6wt% YbB_6 shows the optimal relative density and microhardness, which are 99.43% and 4030 MPa, respectively.

3) The ultimate tensile strength, yield strength, and elongation of the Ti-6Al-4V/ YbB_6 alloys are enhanced due to the formation of TiB and Yb_2O_3 reinforcement phases, grains refinement, and dispersion strengthening. When the 0.6wt% YbB_6 is added into the alloy, the maximum ultimate tensile strength, maximum yield strength, and maximum elongation are 1148 MPa, 903 MPa, and 3.3%, respectively.

4) When the sintering temperature is 1100 °C, the fracture modes of alloys after SPS are mainly the ductile and brittle fracture. When 0.6wt% YbB_6 is added into the alloy, more small dimples appear, and the Yb_2O_3 generated by the in-situ reaction is mainly distributed in the dimples, therefore improving the mechanical properties and fracture toughness of alloys.

References

- Wang X, Wang L, Luo L S et al. *Materials & Design*[J], 2017, 121(5): 335
- Cao Y K, Liu Y, Li Y P et al. *Mechanics of Materials*[J], 2020, 141: 103 260
- Zhu Z S, Wang X N, Shang G Q et al. *Journal of Aeronautical Materials*[J], 2016, 36(3): 7
- Koolu H, Avcu Y Y, Yetik O et al. *Materials Today: Proceedings*[J], 2020, 32: 18
- Liu Y B, Liu Y, Wang B et al. *Advanced Manufacturing Processes*[J], 2010, 25(8): 735
- Jing L L, Li Y H, Cheng K W et al. *IOP Conference Series: Materials Science and Engineering*[C]. Bristol: IOP Publishing, 2020, 740(1): 12 056
- Rastgordani S, Darabi A C, Kadkhodapour J et al. *Surface Topography: Metrology and Properties*[J], 2020, 8(4): 45 016
- Zhang L C, Chen L Y, Wang L. *Advanced Engineering Materials*[J], 2020, 22(5): 1 901 258
- Jiao Y, Huang L J, Wei S L et al. *Corrosion Science*[J], 2018, 140: 223
- Pang W, Man H C, Yue T M. *Materials Science and Engineering A*[J], 2005, 390(1-2): 144
- Variola F, Yi J H, Richert L et al. *Biomaterials*[J], 2008, 29(10): 1285
- Zhang K M, Zou J X, Jun L I et al. *Transactions of the Nonferrous Metals Society of China*[J], 2012, 22(8): 1817
- Gu Yi, Zhang Yuqin, Jiang Yehua et al. *Rare Metal Materials and Engineering*[J], 2014, 43(5): 1238 (in Chinese)
- Hungria T, Galy J, Castro A. *Advanced Engineering Materials*[J], 2009, 11(8): 615
- Tian W M, Li S M, Wang B et al. *International Journal of Minerals, Metallurgy, and Materials*[J], 2016, 23(6): 723
- Falodun O E, Oke S R, Adams F V et al. *Materials Today: Proceedings*[J], 2019, 18(7): 2250
- Auger M A, De Castro V, Leguey T et al. *Journal of Nuclear Materials*[J], 2013, 436(1-3): 68
- Auger M A, Huang Y, Zhang H et al. *Journal of Alloys and Compounds*[J], 2018, 762: 678
- Li W, Xu P Q, Wang Y Y et al. *Journal of Alloys and Compounds*[J], 2018, 749: 10
- Li A, Ma S, Yang Y J et al. *Journal of Alloys and Compounds* [J], 2018, 768: 49
- Chen R, Tan C W, Yu X D et al. *Materials Characterization* [J], 2019, 153: 24
- Li J X, Wang L Q, Qin J N et al. *Materials Science and Engineering A*[J], 2010, 527(21-22): 5811
- Wang S, Luo L M, Zhao M L et al. *Powder Technology*[J], 2016, 294: 301
- Birmingham M J, McDonald S D, Dargusch M S. *Materials Science and Engineering A*[J], 2018, 719: 1
- Yan M, Liu Y, Liu Y B et al. *Scripta Materialia*[J], 2012, 67(5): 491
- Lu W J, Xiao L, Geng K et al. *Materials Characterization* [J], 2008, 59(7): 912
- Menéndez M, Sierra H M, Gent M et al. *Minerals Engineering*[J], 2018, 119: 228
- Hu Z Y, Cheng X W, Li S L et al. *Journal of Alloys and Compounds*[J], 2017, 726: 240
- Habibnejad-Korayem M, Mahmudi R, Poole W J. *Materials Science and Engineering A*[J], 2009, 519(1-2): 198
- Cao F, Chandran K S R, Kumar P. *Scripta Materialia*[J], 2017, 130: 22

YbB₆对Ti-6Al-4V钛合金组织和性能的影响

元想胜^{1,2}, 高春萍^{1,2}, 罗铁钢^{1,3}, 郑雪萍², 李志^{1,3}, 杨杰², 郑子木², 张嘉伟², 罗宇恒⁴

(1. 广东省科学院 新材料研究所, 广东 广州 510650)

(2. 长安大学 材料科学与工程学院, 陕西 西安 710061)

(3. 广东省金属强韧化技术与应用重点实验室, 广东 广州 510650)

(4. 南昌航空大学 环境与化学工程学院, 江西 南昌 330063)

摘要: 采用放电等离子烧结 (SPS) 制备了含YbB₆的Ti-6Al-4V钛合金, 并研究了YbB₆对Ti-6Al-4V钛合金显微组织和力学性能的影响。结果表明, 随着YbB₆含量的增加, 复合材料的显微组织发生转变, 晶粒明显细化, 原位反应生成的TiB晶须和Yb₂O₃颗粒有利于复合材料力学性能的提高。此外, 当添加0.6% (质量分数) YbB₆后, 烧结样品的相对密度、显微硬度、屈服强度、极限拉伸强度和延伸率分别为99.43%、4030 MPa、903 MPa、1148 MPa和3.3%。与Ti-6Al-4V试样相比, 其数值分别提高了0.37%、13.8%、38.07%和17.14%。强化机制主要是组织转变、晶粒细化和弥散强化。随着YbB₆含量的增加, 断裂方式主要为韧性断裂和脆性断裂。

关键词: Ti-6Al-4V; YbB₆; 放电等离子烧结; 微观结构; 机械性能

作者简介: 元想胜, 男, 1996年生, 硕士, 广东省科学院新材料研究所, 广东 广州 510650, E-mail: 18700186983@163.com